Beating the channel capacity limit for linear photonic superdense coding

Julio T. Barreiro, Tzu-Chieh Wei*, and Paul G. Kwiat
Department of Physics, University of Illinois at Urbana-Champaign, Urbana, Illinios 61801-3080, USA
* *Present address: Institute for Quantum Computing and Department of Physics and Astronomy, University of Waterloo, Waterloo, ON N2L 3G1, Canada.*

Dense coding is arguably the protocol that launched the field of quantum communication [1]. Today, however, more than a decade after its initial experimental realization [2], the channel capacity remains fundamentally limited as conceived for photons using linear elements. Bob can only send to Alice three of four potential messages due to the impossibility of performing the deterministic discrimination of all four Bell states with linear optics [3, 4], reducing the attainable channel capacity from 2 to $\log_2 3 \approx 1.585$ bits. However, entanglement in an extra degree of freedom enables the complete and deterministic discrimination of all Bell states [5–7]. Using pairs of photons simultaneously entangled in spin and orbital angular momentum [8, 9], we demonstrate the quantum advantage of the ancillary entanglement. In particular, we describe a dense-coding experiment with the largest reported channel capacity and, to our knowledge, the first to break the conventional linear-optics threshold. Our encoding is suited for quantum communication without alignment [10] and satellite communication.

The first realization of quantum dense coding was optical, using pairs of photons entangled in polarization [2]. Dense coding has since been realized in various physical systems and broadened theoretically to include high-dimension quantum states with multiparties [11], and even coding of quantum states [12]. The protocol extension to continuous variables [13, 14] has also been experimentally explored optically, using superimposed squeezed beams [15]. Other physical approaches include a simulation in nuclear magnetic resonance with temporal averaging [16], and an implementation with atomic qubits on demand without postselection [17]. However, photons remain the optimal carriers of information given their resilience to decoherence and ease of creation and transportation.

Quantum dense coding was conceived [1] such that Bob could communicate two bits of classical information to Alice with the transmission of a single qubit, as follows. Initially, each party holds one spin-$\frac{1}{2}$ particle of a maximally entangled pair, such as one of the four Bell states. Bob then encodes his 2-bit message by applying one of four unitary operations on his particle, which he then transmits to Alice. Finally, Alice decodes the 2-bit message by discriminating the Bell state of the pair.

Alice's decoding step, deterministically resolving the four Bell states, is known as Bell-state analysis (BSA). While in principle attainable with nonlinear interactions, such BSA with photons is very difficult to achieve with present technology, yielding extremely low efficiencies and low discrimination fidelities [18]. Therefore, current fundamental studies and technological developments demand the use of linear optics. However, for quantum communication, standard BSA with linear optics is fundamentally impossible [3, 4]. At best only two Bell states can be discriminated; for quantum communication the other two are considered together for a three-message encoding. Consequently, the maximum channel capacity of this conventional optical dense coding is $\log_2 3 \approx 1.585$ bits. Although there are probabilistic approaches that can distinguish all 4 Bell states (which would be necessary to achieve the fundamental channel capacity of 2), these are at best successful 50% of the time [19], so have a net channel capacity of at most 1 per photon.

Entanglement in an extra degree of freedom (DOF) of the pair, hyperentanglement [20], enables full BSA with linear optics [5, 6]. In this case, since Bob only encodes information in one DOF (the auxiliary DOF is unchanged), a dense-coding protocol proceeds under the same encoding conditions as in the original proposal [1]. Although hyperentanglement-assisted BSA (HBSA) on polarization states has been reported with ancillas entangled in energy-time [6] and linear-momentum [7], no advantage for quantum information or fundamental physics was shown; experiments thus far have been limited to a channel capacity of less than 1.18(3) bits [6], substantially less than is possible even without hyperentangled resources.

Using pairs of photons entangled in their spin and orbital angular momentum (OAM) in a HBSA with high stability and high detection fidelity, we realize a dense-coding experiment with a channel capacity that exceeds the threshold to beat conventional linear-optics schemes. In our scheme, Alice and Bob are provided with pairs of photons simultaneously entangled in their spin and ± 1-OAM in a state of the form

$$\frac{1}{2}(|HH\rangle + |VV\rangle) \otimes (|\circlearrowleft\circlearrowright\rangle + |\circlearrowright\circlearrowleft\rangle). \qquad (1)$$

Here H (V) represents the horizontal (vertical) photon polarization and $\circlearrowleft$ ($\circlearrowright$) represents the paraxial spatial modes (Laguerre-Gauss) carrying $+\hbar$ ($-\hbar$) units of OAM [21]. Bob encodes his message by applying one of four unitary operations on the spin of his photon of this hyperentangled pair: (1) the identity, (2) $V \to -V$, (3) $H \leftrightarrow V$, or (4) $V \to -V$ and $H \leftrightarrow V$. Such operations

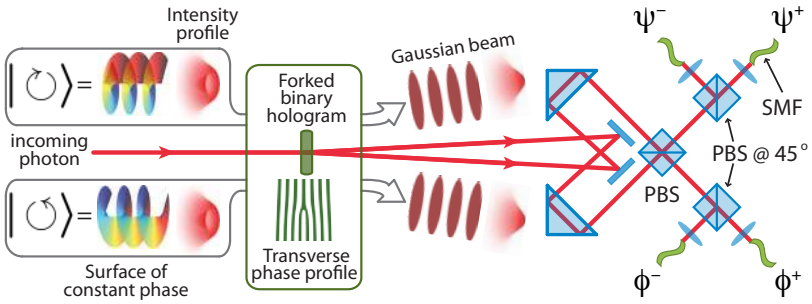

FIG. 1: **Spin-orbit Bell-state analyzer.** A photon in a spin-orbit Bell-state incident from the left is first split according to its ±1-OAM content; its ±1-OAM components are converted to 0-OAM and combined on a polarizing beam splitter (PBS) for a spin-controlled orbit-CNOT gate. The photon is then filtered by a single mode fibre (SMF) and finally routed to a unique detector (photon-counting avalanche photodiode).

transform the state in equation 1 into

$$\Phi^{\pm}_{\text{spin}} \otimes \Psi^{+}_{\text{orbit}}, \text{ and } \Psi^{\pm}_{\text{spin}} \otimes \Psi^{+}_{\text{orbit}}, \tag{2}$$

where the spin and orbit Bell-states are defined as

$$\begin{aligned}
\Phi^{\pm}_{\text{spin}} &\equiv \left(|HH\rangle \pm |VV\rangle\right)/\sqrt{2}, \\
\Psi^{\pm}_{\text{spin}} &\equiv \left(|HV\rangle \pm |VH\rangle\right)/\sqrt{2}, \\
\Psi^{+}_{\text{orbit}} &\equiv \left(|\circlearrowleft\circlearrowleft\rangle + |\circlearrowright\circlearrowright\rangle\right)/\sqrt{2}.
\end{aligned}$$

We designed a HBSA scheme (inspired by Ref. [22]) enabling Alice to discriminate the four states in equation 2. In this scheme, the polarization BSA relies on the observation that the states resulting from Bob's encoding can be rewritten as superpositions of the single-photon Bell-states of spin and orbital angular momentum, or spin-orbit Bell-states:

$$\begin{aligned}
\phi^{\pm} &\equiv \frac{1}{\sqrt{2}}(|H\,\circlearrowleft\rangle \pm |V\,\circlearrowright\rangle), \\
\psi^{\pm} &\equiv \frac{1}{\sqrt{2}}(|H\,\circlearrowright\rangle \pm |V\,\circlearrowleft\rangle).
\end{aligned}$$

In this basis, the states Alice analyzes have the form

$$\begin{aligned}
\Phi^{\pm}_{\text{spin}} \otimes \Psi^{+}_{\text{orbit}} = \frac{1}{2}\big(&\phi_1^{+} \otimes \psi_2^{\pm} + \phi_1^{-} \otimes \psi_2^{\mp} \\
&+ \psi_1^{+} \otimes \phi_2^{\pm} + \psi_1^{-} \otimes \phi_2^{\mp}\big), \\
\Psi^{\pm}_{\text{spin}} \otimes \Psi^{+}_{\text{orbit}} = \frac{1}{2}\big(&\pm\phi_1^{+} \otimes \phi_2^{\pm} \mp \phi_1^{-} \otimes \phi_2^{\mp} \\
&\pm \psi_1^{+} \otimes \psi_2^{\pm} \mp \psi_1^{-} \otimes \psi_2^{\mp}\big).
\end{aligned}$$

This arrangement shows that each hyperentangled state is a unique superposition of four of the sixteen possible combinations of 2-photon spin-orbit Bell-states. Therefore, Alice can decode Bob's message by performing spin-orbit BSA locally on each photon.

We implement the spin-orbit BSA with a novel interferometric apparatus consisting of a ±1-OAM splitter and polarizing beam splitters (PBS), as shown in Fig. 1. The first splitter combines the action of a binary plane-wave phase grating [21] and single-mode fibres. The grating transforms an incoming photon in the state $|\circlearrowleft\rangle$ ($|\circlearrowright\rangle$) into a gaussian beam with no OAM in the +1 (−1) diffraction order (for a splitter that preserves the photon's OAM, see Ref. [21]). Subsequently filtering the first diffraction orders with single-mode fibres, we effectively split an incoming photon into its ±1-OAM components. By merging these diffraction orders on a PBS we perform a spin-controlled NOT gate over the photon OAM. In Fig. 1, the states $\psi^{\pm}$ ($\phi^{\pm}$) exit on the top (bottom) output port of the PBS. Followed by measurements in the diagonal basis, shown in Fig. 1 as PBS@45°, the desired measurement in the single-photon Bell-state basis is accomplished. Additional birefringent elements make this device a universal unitary gate for single-photon two-qubit states, in analogy with the device for polarization-linear momentum states in Ref. [23].

Each step in the dense-coding protocol corresponds to a distinct experimental stage in Fig. 2: a hyperentanglement source, Bob's encoding components, and Alice's HBSA. The hyperentanglement source is realized via spontaneous parametric downconversion in a pair of nonlinear crystals (see Methods section). The generated photon pairs are entangled in polarization, OAM and emission time [9]. In particular, we use a subspace of the produced states which was shown to have a state overlap or fidelity of 97% with the state in equation 1. Next, Bob encodes his message in the polarization state by applying birefringent phase shifts with a pair of liquid crystals, as shown in Fig. 2. Finally, Alice performs HBSA using two of the spin-orbit Bell-state analyzers shown in Fig. 1, one for each photon (see Methods section).

We characterize our dense-coding implementation by switching between the four states for equal intervals, and measuring all output states of the HBSA. The result of these measurements are coincidence counts for each input state, as shown in Fig. 3. From this data we can determine the conditional detection probabilities that Alice detects each message $\Phi^{\pm}$ and $\Psi^{\pm}$ given that Bob sent, for example, the message Φ^{+}. The probabilities shown

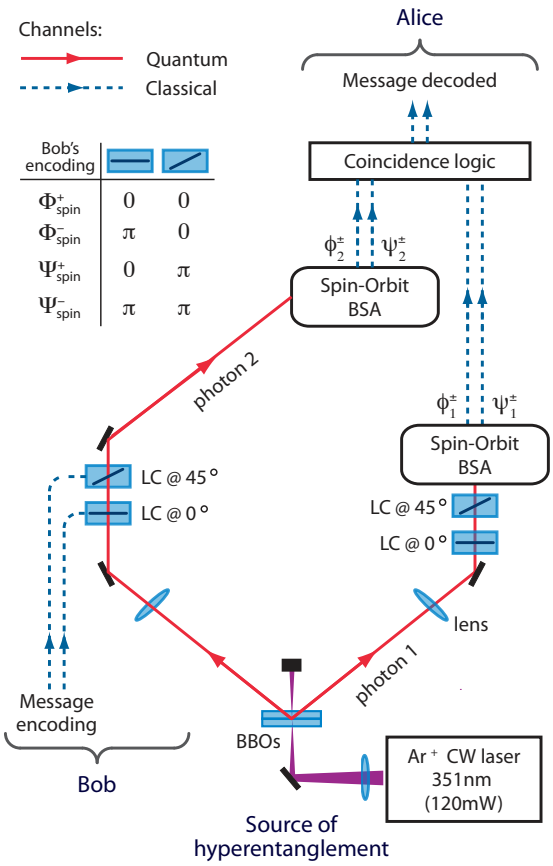

FIG. 2: **Experimental setup for dense coding with spin-orbit encoded photons.** Acting on photon 2 of a hyperentangled pair, Bob encodes his message by using the liquid crystals (LCs) to apply the phases indicated in the table, while (or earlier) Alice performs spin-orbit BSA on photon 1. Later –the upward direction suggests time progression– Alice uses a spin-orbit BSA on photon 2, and the result from the measurement on photon 1, to decode Bob's message. The liquid crystals on the path of photon 1 applied no phase during the dense-coding experiment, but were used along with Bob's liquid crystals to characterize the polarization states of the hyperentangled source by quantum state tomography. The liquid-crystal optic axes are perpendicular to the incident beams; LC@45° (LC@0°) is oriented at 45° (0°) from the horizontal polarization direction. BBOs: β-barium borate nonlinear crystals; CW: continuous-wave.

in Fig. 4 were calculated by comparing the sum of the four rates corresponding to each detected message over the sum of all sixteen rates for the sent message. The average probability of success was 94.8(2)% (all reported errors from Monte Carlo simulations).

A better figure of merit for a quantum dense-coding implementation is the channel capacity, since it characterizes the exponential growth of the maximum number of distinguishable signals for a given number of uses of the channel (see Methods section). From the conditional detection probabilities, we obtain a channel capacity of 1.630(6) bits with a probability of sending each state of $P(\Phi^+) = 0.26$, $P(\Phi^-) = 0.26$, $P(\Psi^+) = 0.24$, and $P(\Psi^-) = 0.24$. This exceeds the 1.585 channel-capacity threshold for conventional linear-optics implementations. The channel capacity drifted by no more than one standard deviation between experimental runs, demonstrating the high stability of the implementation.

The experimental channel capacity is nevertheless smaller than the maximum attainable (2 bits), due to imperfections in the alignment, input states and components. By characterizing each imperfection and modelling the gates and measurement, we estimated their effect on the channel capacity (see Supplementary Information II). Considering all mentioned imperfections (see Methods section) and their spread in a Monte Carlo simulation, the predicted channel capacity of 1.64(2) bits agrees with the measured channel capacity of 1.630(6) bits. The polarization and spatial-mode states can be improved by spatially compensating the angle-dependent phase [24], using a forked hologram with a smaller diffraction angle to decrease wavelength dispersion (a potential source of alignment imbalances), and obtaining crystals with a smaller wedge. The deleterious effect of the PBS crosstalk can be reduced by adding extra phase-compensation plates inside the interferometers, and can potentially be eliminated altogether by adding appropriate birefringent beam displacers after each PBS.

Above, Bob encoded two qubits in the form of spin-orbit Bell-states by acting only on the spin DOF. However, more generally he could also apply one of four unitaries in the ± 1-OAM subspace and encode four qubits. The state of the pair of photons then becomes a product of Bell states, 16 in total. In principle, if Alice could discriminate all these "hyper-Bell" states, up to 4 bits could be transmitted per photon. We have investigated the limits for unambiguously distinguishing these Bell-like states, and have found that the optimal one-shot discrimination scheme is to group the 16 states into 7 distinguishable classes [25]. The optimal analysis can be achieved by the Kwiat-Weinfurter scheme [5], with photon-number resolving detectors, giving a maximum channel capacity of $\log_2 7 \approx 2.81$ bits. If we modify the present scheme, we can also implement an unambiguous discrimination of all 16 Bell states with two identical copies [25].

In conclusion, we have beaten a fundamental limit on the channel capacity for standard dense coding using only linear optics. A number of features make our HBSA efficient and reliable. First, hyperentanglement offers advantages in the source, logic gates and detection side. Quantum logic between qubits encoded on different DOFs is much more easily implemented than when using different photons [26, 27]. From the source side, more quantum information is available per photon, particularly with the energy-time and spatial-mode DOF(e.g., [28]). In the detection side, compared to multi-photon approaches, higher efficiency is achieved because only one

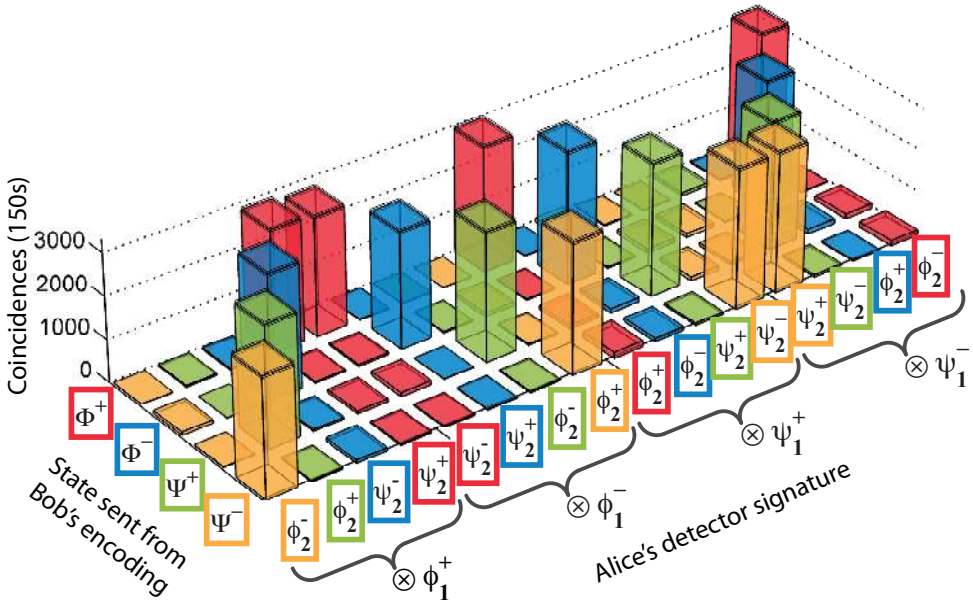

FIG. 3: **Experimental results of hyperentanglement-assisted dense coding.** Coincidence counts detected by Alice's HBSA for each message (state) sent by Bob. The error bars (shown as additional squares at the top of each column) represent ±1 standard deviations, deduced from poissonian counting statistics. The state-discrimination signal-to-noise ratios (SNR), which compare the sum of the four rates corresponding to the actual state to the sum of the other twelve registered rates, are $SNR_{\Phi^+} = 19.9(8)$, $SNR_{\Phi^-} = 27(1)$, $SNR_{\Psi^+} = 13.7(5)$, and $SNR_{\Psi^-} = 16.4(6)$.

pair of photons is detected. Second, since our HBSA requires only local measurements, Alice can measure one of the photons and store the classical result of her measurement until Bob sends his photon (i.e., she does not require a quantum memory). Finally, the photon's polarization and ±1-OAM constitute a robust encoding as they enable quantum communication without alignment [10] as well as other landmark advances for quantum information [8]. Furthermore, by using paraxial beams as the ancillary DOF, the scheme is free of tight source-to-detector requirements such as interferometric stability [7] or perfect indistiguishability for HOM interference [6]. However, OAM single-photon and entangled states easily decohere by atmospheric turbulence [29, 30], limiting their likely communication applications to satellite-to-satellite transmissions.

METHODS

The hyperentanglement source is realized by directing 120 mW of 351 nm light from a continuous-wave (CW) Ar^+ laser into two contiguous β-barium borate (BBO) nonlinear crystals with optic axes aligned in perpendicular planes [9]. Type-I degenerate 702 nm photons in a 3.0° half-opening angle cone are produced by phase-matching each 0.6-mm-thick crystal. In the spin and ±1 OAM subspace, a two-fold coincidence rate of 5 detected pairs/s is determined by a 10 ns coincidence window and interference filters with $\Delta\lambda_{\mathrm{FWHM}} = 5$ nm.

In our HBSA implementation each PBS@45° and its two outputs in the spin-orbit BSA (Fig. 1) were replaced by a dichroic polarizer oriented at either 45° or −45° and a single output; Alice's HBSA thus acquires all spin-orbit BSA outputs from four polarizer settings. With the CW source, Alice cycles through the four polarizer settings, and for each polarizer setting Bob encodes the four messages, each for 150 seconds. During the measurement, no active stabilization or realignment was done on the source, spin-orbit BSA interferometers, or coupling optics. The HBSA polarizers and liquid crystals were quickly set with computer-controlled rotation stages and liquid crystal controllers.

The wavelength-dependent voltage applied to each liquid crystal was independently calibrated to produce a birefringent phase difference of 0 or π with a diode laser operated at 699 nm (Hitachi HL-6738MG, driven at 140mA and 80°C); the same laser was used to align the ±1-OAM splitter. The binary forked holograms were silver-halide emulsion gratings with 33%-diffraction efficiency into the first order (more efficient schemes are described in Ref. [21]). The same holographic plate included spatial-mode tomography patterns, which in conjunction with the liquid crystals were used for state reconstruction [9]. The spurious phase upon reflection on the PBS was compensated with a waveplate in each output port of the PBS for both spin-orbit Bell-state analyzers. The state discrimination signal-to-noise ration (SNR) varied between states due to mode-coupling im-

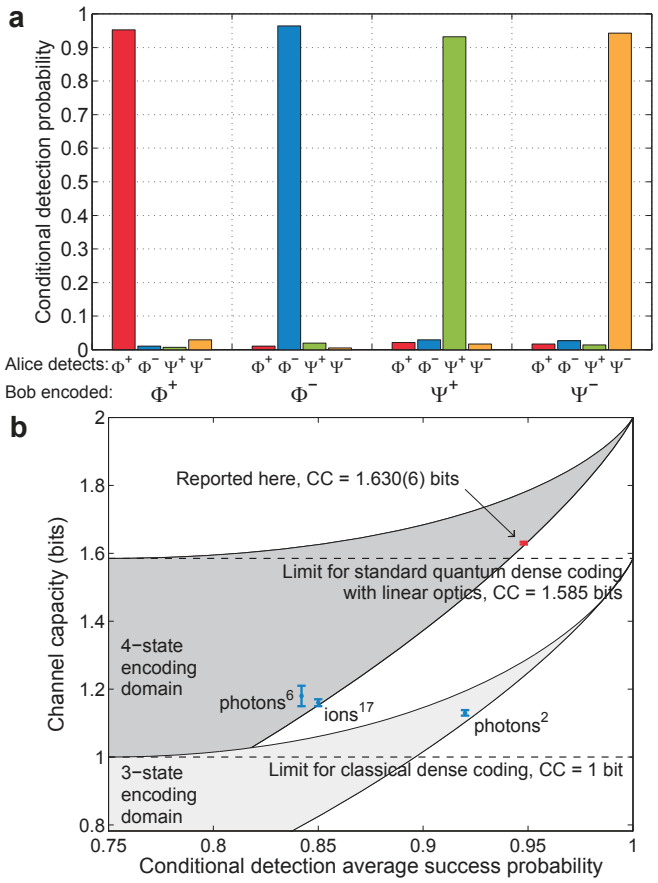

FIG. 4: **Conditional detection probabilities beating the channel capacity limit for standard dense-coding with linear optics. a** Given that Bob encoded the four states indicated, Alice infers the state transmitted with the probabilites shown (calculated from data in Fig. 3). Her average success probability is 94.8(2)%. The uncertainty in each probability is less than 0.2%. These results imply a channel capacity of 1.630(6) bits, above the standard linear-optics limit of 1.585. **b** Experimentally reported channel capacities as a function of their conditional detection average success probability. The error bars represent the statistical error of ±1 standard deviations. The domains of achievable channel capacity for both 3- and 4-state encodings are shown for reference (see Supplementary Information I).

balance in the spin-orbit BSA, PBS crosstalk, and slight offsets in the liquid crystal calibrations.

We characterized the source polarization state $\Phi^-_{\rm spin}$ by quantum state tomography in the $|\circlearrowleft\circlearrowleft\rangle$ and $|\circlearrowright\circlearrowright\rangle$ OAM subspaces [9] (using the liquid crystals shown in Fig. 2 and PBS of each spin-orbit BSA shown in Fig. 1). Considering all combinations of signature detectors, we measured an average degree of entanglement or tangle of $T = 96.7(8)\%$ and a mixture or linear entropy of $S_L = 2.0(4)\%$. If such high-quality polarization state were exactly the same for each combination of signature detectors, the decrease in the channel capacity would only be 0.006 bits. However, small differences in the coupled state between each combination of detectors (expressed above as uncertainty) result in a channel capacity decrease of 0.09(2) (see Supplementary Information II). The OAM state was also tomographically reconstructed in the $|HH\rangle$ and $|VV\rangle$ polarization subspaces [9], measuring an average $T = 91(3)\%$ and $S_L = 6(2)\%$, yielding a channel capacity decrease of 0.20(3) bits. The PBS crosstalk (0.5% for H, 1.0% for V) further decreases the channel capacity by 0.10(1) bits. Finally, accidental coincidences (5 in 150s) reduce channel capacity by 0.02 bits.

Channel capacity

The capacity of a noisy channel is given by $\max_{p(x)} H(X:Y)$, where x is in the space of signals that can be transmitted X, $H(X:Y)$ is the mutual information of X and the space of received signals Y, and the maximum is taken over all input distributions $p(x)$. $H(X:Y)$ is a function of $p(x)$ and the conditional detection distribution $p(y|x)$ of receiving y given that x was sent:

$$H(X:Y) = \sum_{y\in Y}\sum_{x\in X} p(x)p(y|x)\log\frac{p(y|x)}{\sum_{x\in X}p(y|x)p(x)}.$$

In our experiment, a uniform probability of transmission gives a mutual information of 1.629(6) bits, negligibly smaller than the channel capacity due to the nearly balanced conditional probabilities, i.e., there is little to be gained by sending some states more frequently.

Correspondence and requests for materials should be addressed to J.T.B. e-mail: julio.barreiro@gmail.com

ACKNOWLEDGEMENTS

We thank N. Peters and N. Langford for helpful discussions and R. Hillmer for assistance in hologram fabrication. This work was jointly supported by the DTO/ARO-sponsored MURI Center for Photonic Quantum Information Systems, and the DTO/IARPA-sponsored Advanced Quantum Communication grant. J.T.B. acknowledges support from CONACYT-México.

Supplementary Information accompanies this paper.

COMPETING FINANCIAL INTERESTS

The authors declare no competing financial interests.

[1] Bennett, C. H. & Wiesner, S. J. Communication via one- and two- particle operators on Einstein-Podolsky-Rosen states. *Phys. Rev. Lett.* **69,** 2881–2884 (1992).

[2] Mattle, K. *et al.* Dense coding in experimental quantum communication. *Phys. Rev. Lett.* **76,** 4656–4659 (1996).

[3] Vaidman, L. & Yoran, N. Methods for reliable teleportation. *Phys. Rev. A* **59,** 116–125 (1999).

[4] Lütkenhaus, N., Calsamiglia, J. & Suominen, K. A. Bell measurements for teleportation. *Phys. Rev. A* **59,** 3295–3300 (1999).

[5] Kwiat, P. G. & Weinfurter, H. Embedded Bell-state analysis. *Phys. Rev. A* **58,** R2623–R2626 (1998).

[6] Schuck, C., Huber, G., Kurtsiefer, C. & Weinfurter, H. Complete deterministic linear optics Bell state analysis. *Phys. Rev. Lett.* **96,** 190501 (2006).

[7] Barbieri, M., Vallone, G., Mataloni, P. & Martini, F. D. Complete and deterministic discrimination of polarization Bell states assisted by momentum entanglement. *Phys. Rev. A* **75,** 042317 (2007).

[8] Molina-Terriza, G., Torres, J. P. & Torner, L. Twisted photons. *Nature Physics* **3,** 305–310 (2007).

[9] Barreiro, J. T., Langford, N. K., Peters, N. A. & Kwiat, P. G. Generation of hyperentangled photon pairs. *Phys. Rev. Lett.* **95,** 260501 (2005).

[10] Aolita, L. & Walborn, S. P. Quantum communication without alignment using multiple-qubit single-photon states. *Phys. Rev. Lett.* **98,** 100501 (2007).

[11] Liu, X. S., Long, G. L., Tong, D. M. & Li, F. General scheme for superdense coding between multiparties. *Phys. Rev. A* **65,** 022304 (2002).

[12] Harrow, A., Hayden, P. & Leung, D. Superdense coding of quantum states. *Phys. Rev. Lett.* **92,** 187901 (2004).

[13] Braunstein, S. L. & Kimble, H. J. Dense coding for continuous variables. *Phys. Rev. A* **61,** 042302 (2000).

[14] Ban, M. Quantum dense coding via a two-mode squeezed-vacuum state. *J. Opt. B: Quantum Semiclass. Opt.* **1,** L9 (1999).

[15] Li, X. *et al.* Quantum dense coding exploiting a bright Einstein-Podolsky-Rosen beam. *Phys. Rev. Lett.* **88,** 047904 (2002).

[16] Fang, X., Zhu, X., Feng, M., M, X. & Du, F. Experimental implementation of dense coding using nuclear magnetic resonance. *Phys. Rev. A* **61,** 022307 (2000).

[17] Schaetz, T. *et al.* Quantum dense coding with atomic qubits. *Phys. Rev. Lett.* **93,** 040505 (2004).

[18] Kim, Y.-H., Kulik, S. P. & Shih, Y. Quantum teleportation of a polarization state with a complete Bell state measurement. *Phys. Rev. Lett.* **86,** 1370–1373 (2001).

[19] Calsamiglia, J. & Lutkenhaus, N. Maximum efficiency of a linear-optical Bell-state analyzer. *Appl. Phys. B: Lasers Opt.* **B72,** 67–71 (1999).

[20] Kwiat, P. G. Hyper-entangled states. *J. Mod. Opt.* **44,** 2173–2184 (1997).

[21] Allen, L., Barnett, S. M. & Padgett, M. J. (eds.) *Optical Angular Momentum* (Institute of Physics Publishing, Bristol, 2003).

[22] Walborn, S. P., Pádua, S. & Monken, C. H. Hyperentanglement-assisted Bell-state analysis. *Phys. Rev. A* **68,** 042313 (2003).

[23] Englert, B.-G., Kurtsiefer, C. & Weinfurter, H. Universal unitary gate for single-photon two-qubit states. *Phys. Rev. A* **63,** 032303 (2001).

[24] Altepeter, J. B., Jeffrey, E. R. & Kwiat, P. G. Phase-compensated ultra-bright source of entangled photons. *Opt. Express* **13,** 8951–8959 (2005).

[25] Wei, T.-C., Barreiro, J. T. & Kwiat, P. G. Hyperentangled Bell-state analysis. *Phys. Rev. A* **75,** 060305(R) (2007).

[26] Cerf, N. J., Adami, C. & Kwiat, P. G. Optical simulation of quantum logic. *Phys. Rev. A* **57,** R1477–R1480 (1998).

[27] Fiorentino, M. & Wong, F. N. C. Deterministic controlled-not gate for single-photon two-qubit quantum logic. *Phys. Rev. Lett.* **93,** 070502 (2004).

[28] Ali-Khan, I., Broadbent, C. J. & Howell, J. C. Large-alphabet quantum key distribution using energy-time entangled bipartite states. *Phys. Rev. Lett.* **98,** 060503 (2007).

[29] Paterson, C. Atmospheric turbulence and orbital angular momentum of single photons for optical communication. *Phys. Rev. Lett.* **94,** 153901 (2005).

[30] Smith, B. J. & Raymer, M. G. Two-photon wave mechanics. *Phys. Rev. A* **74,** 062104 (2006).

Beating the channel capacity limit for linear photonic superdense coding
SUPPLEMENTARY INFORMATION

Julio T. Barreiro, Tzu-Chieh Wei, and Paul G. Kwiat
Department of Physics, University of Illinois at Urbana-Champaign, Urbana, Illinois 61801-3080, USA

SUPPLEMENT I: CHANNEL CAPACITY AS A FUNCTION OF CONDITIONAL DETECTION AVERAGE SUCCESS PROBABILITY (FIGURE 4B)

In Fig. 4**b**, the channel capacity upper bound for the 4-state encoding domain occurs when two of the four states are faithfully transmitted and the other two mixed, corresponding to a transfer matrix of conditional probabilities $p(y|x)$ of receiving the state y given that the state x was sent,

$$\begin{pmatrix} p(\Phi^+|\Phi^+) & p(\Phi^+|\Phi^-) & p(\Phi^+|\Psi^+) & p(\Phi^+|\Psi^-) \\ p(\Phi^-|\Phi^+) & p(\Phi^-|\Phi^-) & p(\Phi^-|\Psi^+) & p(\Phi^-|\Psi^-) \\ p(\Psi^+|\Phi^+) & p(\Psi^+|\Phi^-) & p(\Psi^+|\Psi^+) & p(\Psi^+|\Psi^-) \\ p(\Psi^-|\Phi^+) & p(\Psi^-|\Phi^-) & p(\Psi^-|\Psi^+) & p(\Psi^-|\Psi^-) \end{pmatrix} = \begin{pmatrix} 2p_s-1 & 2(1-p_s) & 0 & 0 \\ 2(1-p_s) & 2p_s-1 & 0 & 0 \\ 0 & 0 & 1 & 0 \\ 0 & 0 & 0 & 1 \end{pmatrix} \tag{1}$$

with an input distribution $p(x)$ maximized for each conditional detection average success probability p_s. The lower bound is set by a uniform noise over the failed transmissions, resulting in a transfer matrix:

$$\begin{pmatrix} p_s & f & f & f \\ f & p_s & f & f \\ f & f & p_s & f \\ f & f & f & p_s \end{pmatrix}, \tag{2}$$

where $f = (1-p_s)/3$ and for all sent messages x, the input distribution that maximizes the mutual information is $p(x) = 1/4$.

SUPPLEMENT II: EFFECT OF EXPERIMENTAL IMPERFECTIONS ON THE CHANNEL CAPACITY

In our scheme, the major detriments to the channel capacity are the input polarization and spatial-mode states and the PBS crosstalk; accidental coincidences lead to only a minor CC reduction. We model each imperfection as a function of relevant parameters, which were estimated by quantum state tomography or measured. Then we feed these parameters into a Monte Carlo simulation of the expected channel capacity, as described below.

Modelling imperfections: The input states

The imperfections in the hyperentangled state generated by spontaneous parametric downconversion, $|\Phi^-_{\rm spin}\rangle \otimes |\Psi^+_{\rm orbit}\rangle$ in our case, can be modelled with high fidelity by uniform-noise decoherence, a population imbalance angle ϵ_θ and a relative phase ϵ_ϕ. The deviations from the ideal pure state $|\Phi^-_{\rm spin}\rangle \otimes |\Psi^+_{\rm orbit}\rangle$ have the following form

$$|\Phi^-_{\rm spin}(\epsilon_{\theta,\rm spin}, \epsilon_{\phi,\rm spin})\rangle = \cos(\pi/4+\epsilon_{\theta,\rm spin})|HH\rangle - e^{i\epsilon_{\phi,\rm spin}}\sin(\pi/4+\epsilon_{\theta,\rm spin})|VV\rangle, \tag{3}$$

$$|\Psi^+_{\rm orbit}(\epsilon_{\theta,\rm orbit}, \epsilon_{\phi,\rm orbit})\rangle = \cos(\pi/4+\epsilon_{\theta,\rm orbit})|\circlearrowleft\circlearrowleft\rangle + e^{i\epsilon_{\phi,\rm orbit}}\sin(\pi/4+\epsilon_{\theta,\rm orbit})|\circlearrowright\circlearrowright\rangle. \tag{4}$$

The uniform-noise decoherence is characterized by a parameter λ and it adds mixture to each spin and orbital density matrices in the form $\rho(\lambda) = (1-\lambda)\rho + \lambda \mathbf{I}_4$, where $\mathbf{I}_4$ is the 4-dimensional identity matrix. Since the imperfections also affect the messages encoded, the four states in the dense-coding protocol have a functional dependence on the source parameters ϵ_θ, ϵ_ϕ and λ:

$$\begin{aligned} &\Phi^\pm_{\rm spin}(\epsilon_{\theta,\rm spin}, \epsilon_{\phi,\rm spin}, \lambda_{\rm spin}) \otimes \Psi^+_{\rm orbit}(\epsilon_{\theta,\rm orbit}, \epsilon_{\phi,\rm orbit}, \lambda_{\rm orbit}) \\ &\Psi^\pm_{\rm spin}(\epsilon_{\theta,\rm spin}, \epsilon_{\phi,\rm spin}, \lambda_{\rm spin}) \otimes \Psi^+_{\rm orbit}(\epsilon_{\theta,\rm orbit}, \epsilon_{\phi,\rm orbit}, \lambda_{\rm orbit}) \end{aligned} \tag{5}$$

Moreover, since these parameters vary slightly due to alignment [1] and component imperfections among the different combinations of signature detectors, we performed a quantum state tomography in each combination and determined the spread in the parameters. To estimate the channel capacity, we performed Monte Carlo simulations where the above parameters are the random variables following a normal distribution with a standard deviation given by the spread of the estimated parameters.

Modelling imperfections: The spin-orbit gate

The forked hologram maps the OAM states $|\circlearrowleft\rangle$ and $|\circlearrowright\rangle$ into distinct propagation modes a and b with no OAM, respectively corresponding to the $+1$ and -1 diffraction orders (with a π phase shift difference):

$$\begin{pmatrix} |H\circlearrowleft\rangle \\ |H\circlearrowright\rangle \\ |V\circlearrowleft\rangle \\ |V\circlearrowright\rangle \end{pmatrix} \xmapsto{\text{forked hologram}} \begin{pmatrix} |H_a\rangle \\ -|H_b\rangle \\ |V_a\rangle \\ -|V_b\rangle \end{pmatrix}. \tag{6}$$

The polarizer beam splitter (PBS) is modelled with a crosstalk parameter for each polarization, ϵ_H and ϵ_V, and a relative phase shift between H and V polarizations for each output mode, ϕ_1 and ϕ_2. In the basis of Eq. 6,

$$PBS(\epsilon_H,\epsilon_V,\phi_1,\phi_2) = \begin{pmatrix} \sqrt{1-\epsilon_H} & -\sqrt{\epsilon_H} & 0 & 0 \\ \sqrt{\epsilon_H} & \sqrt{1-\epsilon_H} & 0 & 0 \\ 0 & 0 & e^{\frac{1}{2}i(\phi_1+\phi_2)}\sqrt{\epsilon v} & -e^{i\phi_2}\sqrt{1-\epsilon v} \\ 0 & 0 & e^{i\phi_1}\sqrt{1-\epsilon v} & e^{\frac{1}{2}i(\phi_1+\phi_2)}\sqrt{\epsilon v} \end{pmatrix}. \tag{7}$$

The phase shifts ϕ_1 and ϕ_2 were corrected with tilted birefringent plates (quarter-wave plates, in particular) with their optic axes aligned parallel to the direction of horizontal polarization. Therefore, for the model we can set $\phi_1 = \phi_2 = 0$, and the PBS depends only on the crosstalk, $PBS(\epsilon_H, \epsilon_V)$.

The gate for the pair of photons is therefore

$$U(\epsilon_H,\epsilon_V) = \left(PBS(\epsilon_H,\epsilon_V)\cdot \text{Hologram}\right)_{\text{photon 1}} \otimes \left(PBS(\epsilon_H,\epsilon_V)\cdot \text{Hologram}\right)_{\text{photon 2}}. \tag{8}$$

Estimating the channel capacity

Using the above input states and spin-orbit gates we can estimate the conditional detection probabilities; for example, the probability of inferring Φ^+ given that Φ^- was sent is

$$p(\Phi^+|\Phi^-) = \langle \Phi^+_{\text{spin}} \otimes \Psi^+_{\text{orbit}} | U(\epsilon_H,\epsilon_V) \rho_{\Phi^-_{\text{spin}}\otimes\Psi^+_{\text{orbit}}} U(\epsilon_H,\epsilon_V)^\dagger | \Phi^+_{\text{spin}} \otimes \Psi^+_{\text{orbit}} \rangle, \tag{9}$$

where $\rho_{\Phi^-_{\text{spin}}\otimes\Psi^+_{\text{orbit}}}$ is a function of $\epsilon_{\theta,\text{spin}}$, $\epsilon_{\phi,\text{spin}}$, λ_{spin}, $\epsilon_{\theta,\text{orbit}}$, $\epsilon_{\phi,\text{orbit}}$ and λ_{orbit}. Finally, the channel capacity is obtained by maximizing the mutual information over all the input distributions.

Results

We characterized the source polarization state Φ^-_{spin} by quantum state tomography in the $|\circlearrowleft\circlearrowright\rangle$ and $|\circlearrowright\circlearrowright\rangle$ OAM subspaces [2]. Considering all combinations of signature detectors, we measured an average degree of entanglement or tangle of $T = 96.7(8)\%$ and a mixture or linear entropy of $S_L = 2.0(4)\%$. The OAM state was also tomographically reconstructed in the $|HH\rangle$ and $|VV\rangle$ polarization subspaces [2], measuring an average $T = 91(3)\%$ and $S_L = 6(2)\%$. We calculated the states of the form of Eq. 3 and 4 closest to the reconstructed density matrices. The fidelity between the reconstructed and closest estimated states is 99% for polarization and 97% for spatial-mode states. The estimated parameters and their spread are shown in the table below. The achievable channel capacity under only one imperfection is quoted as well. The Monte Carlo simulations used 100 iterations, enough to display stable values in the first digit of the uncertainty.

Imperfection	Conditional detection average success probability	Achievable CC (bits)	CC reduction (bits)
Source polarization state $\epsilon_{\theta,\mathrm{spin}} = 1.0(7)^\circ$, $\epsilon_{\phi,\mathrm{spin}} = 0(4)^\circ$, $\lambda_{\mathrm{spin}} = 0.010(2)$ $T = 96.7(8)\%$, $S_L = 2.0(4)\%$	0.991(2)	1.91(2)	0.09(2)
Source spatial-mode state $\epsilon_{\theta,\mathrm{orbit}} = 1.7(6)^\circ$, $\epsilon_{\phi,\mathrm{orbit}} = 0(5)^\circ$, $\lambda_{\mathrm{orbit}} = 0.03(1)$ $T = 91(3)\%$, $S_L = 6(2)\%$	0.971(4)	1.80(3)	0.20(3)
PBS crosstalk $\epsilon_H = 0.005(1)$, $\epsilon_V = 0.010(2)$	0.985(2)	1.90(1)	0.10(2)
Accidentals (5 in 150s)	0.998(1)	1.98(1)	0.02(1)
All the above imperfections in the same simulation	0.953(3)	1.64(2)	0.36(2)

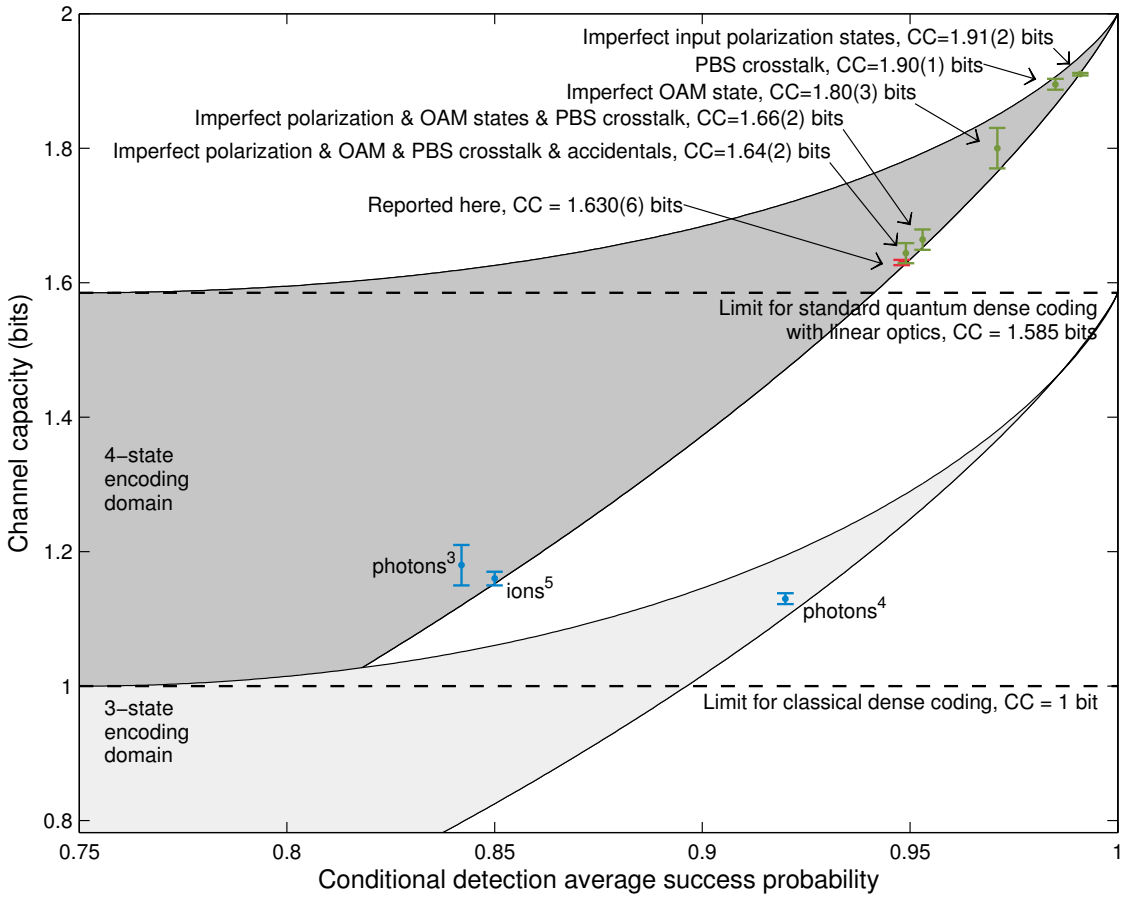

FIG. 1: **Experimentally achieved and simulated channel capacities as a function of conditional detection average success probability.** The simulated CC for our hyperentanglement-assisted dense-coding protocol, when affected by only the experimental imperfections indicated, are shown in green. The CC reported in the accompanying article is shown in red. Previously reported CCs are shown in blue for photons with [3] and without hyperentanglement [4] and for ions [5].

The subtle and convoluted character of the imperfections is evident upon directly adding the independently modeled CC reductions of each imperfection, which would predict an anomalously low CC=1.59 bits, compared to the full Monte-Carlo simulation resulting from simultaneously modelling all the effects, which predicts CC=1.64(2) bits.

Finally, we stress that the reported conditional distribution was not normalized by the statistical detection probabilities to account for detection imbalances over the different states; these were well balanced in our case, only 3% off for the states Φ^- and Ψ^+, such normalization would increase our reported CC to 1.634(6) bits.

[1] For example, the input polarization state phase ϕ depends on the collection angle [6], resulting in small but different phases for each coupling combination.
[2] Barreiro, J. T., Langford, N. K., Peters, N. A. & Kwiat, P. G. Generation of hyperentangled photon pairs. *Phys. Rev. Lett.* **95**, 260501 (2005).
[3] Schuck, C., Huber, G., Kurtsiefer, C. & Weinfurter, H. Complete deterministic linear optics Bell state analysis. *Phys. Rev. Lett.* **96**, 190501 (2006).
[4] Mattle, K. *et al.* Dense coding in experimental quantum communication. *Phys. Rev. Lett.* **76**, 4656–4659 (1996).
[5] Schaetz, T. *et al.* Quantum dense coding with atomic qubits. *Phys. Rev. Lett.* **93**, 040505 (2004).
[6] Altepeter, J. B., Jeffrey, E. R. & Kwiat, P. G. Phase-compensated ultra-bright source of entangled photons. *Opt. Express* **13**, 8951–8959 (2005).